Journal of Physics: Condensed Matter

PAPER

High-pressure synthesis and characterizations of a new ternary Ce-based compound Ce_3TiAs_5

IOP Publishing Journal of Physics: Condensed Matter
J. Phys.: Condens. Matter **37** (2025) 015803 (8pp) https://doi.org/10.1088/1361-648X/ad7fb4

High-pressure synthesis and characterizations of a new ternary Ce-based compound Ce_3TiAs_5

L C Fu[1,2], L C Shi[1,3], X M Chen[1,4], L Duan[4], Y Peng[1,3], J Zhang[1], J Song[1], Z Deng[1], S J Zhang[1], J F Zhao[1], Y Liu[5], J F Zhang[1], J L Zhu[2,5,*], X C Wang[1,3,*] and C Q Jin[1,3,*]

[1] Beijing National Laboratory for Condensed Matter Physics, Institute of Physics, Chinese Academy of Sciences, Beijing 100190, People's Republic of China
[2] Department of Physics, Southern University of Science and Technology, Shenzhen 518055, People's Republic of China
[3] School of Physics, University of Chinese Academy of Sciences, Beijing 100190, People's Republic of China
[4] School of Materials Science and Engineering, Henan University of Technology, Zhengzhou 450007, People's Republic of China
[5] Quantum Science Center of Guangdong-Hong Kong-Macao Greater Bay Area (Guangdong), Shenzhen 518045, People's Republic of China

E-mail: zhujl@sustech.edu.cn, wangxiancheng@iphy.ac.cn and jin@iphy.ac.cn

Received 5 June 2024, revised 16 September 2024
Accepted for publication 25 September 2024
Published 14 October 2024

Abstract

We report the structure and properties of a new Ce-based compound Ce_3TiAs_5 synthesized under high-pressure and high-temperature conditions. It crystallizes in a hexagonal Hf_5Sn_3Cu-anti type structure with zig-zag like Ce chains along the c axis. This compound is metallic and undergoes a magnetic phase transition at $T_N = 13$ K. A metamagnetic transition occurs at ~0.7 T. The Sommerfeld coefficient for the compound is determined to be about 215 mJ/(Ce-mol*K^2), demonstrating a heavy Fermion behavior. The resistivity is featured with two humps, which arises from the synergistic effect of crystal electric field and magnetic scattering. The magnetic ordering temperature T_N gradually increases in the sequence of Ce_3TiPn_5 with Pn = Bi, Sb, and As, which implies that the Ruderman–Kittel–Kasuya–Yosida interaction should be still predominant in Ce_3TiAs_5.

Keywords: Kondo effect, magnetism, heavy fermion, quasi 1D structure

1. Introduction

Ce-based compounds have attracted many research interests since the discovery of the unconventional superconductor $CeCu_2Si_2$ [1–9]. They exhibit rich physical phenomena, such as magnetism with different magnetic structures, heavy fermion superconductivity (SC) and quantum critical behavior. These physical properties of Ce-based compounds are commonly governed by the competition between magnetic Ruderman–Kittel–Kasuya–Yosida (RKKY) interaction and Kondo effect and can be well described by the Doniach's phase diagram [10]. Both the strength of RKKY interaction and Kondo effect depends on the coupling between conducting electrons and Ce–4f electrons (c–f coupling J_0) but with different functional relationship. For a weak J_0, the ground state is mostly governed by the RKKY interactions, resulting in a magnetic ordering ground state. While with increasing J_0, the Kondo effect would gradually become the dominant one and lead to the suppression of magnetic ordering. The system will reach a quantum critical point when the magnetic ordering is fully suppressed, near which heavy fermion SC usually

* Authors to whom any correspondence should be addressed.

is observed. For example, $CeCu_2Si_2$ locates near the quantum critical point and exhibit SC with a very large Sommerfeld coefficient $\gamma \sim 1000$ mJ/(mol*K^2) under ambient pressure [1]. As J_0 can be enhanced through applying physical pressure, some Ce-based compounds also show the pressure-induced SC near the quantum critical point, like $CeRh_2Si_2$ and $CeRhIn_5$ [11–13].

Recently, two heavy fermion compounds Ce_3TiPn_5 (Pn denotes the pnictogen of Sb/Bi) have been reported with a large Sommerfeld coefficient close to 200 mJ/(Ce-mol*K^2) [14, 15]. They crystallize in a hexagonal structure with the space group of $P6_3/mcm$, where the Ce atoms locate on the 6 g site and form a zig-zag like chain along the c-axis. Both of the compounds undergo antiferromagnetic (AFM) transition with an easy ab-plane at T_N about 5.0 K and 5.5 K for Ce_3TiBi_5 and Ce_3TiSb_5, respectively [14–16]. Ce_3TiBi_5 forms a cycloid order with the propagation vector $k = (0, 0, 0.386)$ and spin moments lying in the plane containing the Ce zig-zag chain [17], while Ce_3TiSb_5 has two coexisting magnetic structures with $k_1 = (0, 1/2, 1/8)$ and $k_2 = (0, 0, 1/8)$ and moments lying perpendicular to the zig-zag-chain plane [18]. Their resistivity curves are featured with broad hump near 100 K, suggesting the interplay of crystal electric field (CEF) and magnetic scattering [14, 19].The AFM tuned by pressure for Ce_3TiBi_5 has been studied. The T_N value is initially increased by pressure to a maximum of ~10.2 K at 6 GPa, after which it goes down with further increasing pressure [20]. Up to now, there is no report about the As-based Ce_3TiPn_5 compound. Since the As atomic size is small relative to Sb/Bi, the replacement of Sb/Bi by As in Ce_3TiSb/Bi_5 can be considered as a positive chemical pressure and thus make it possible to study the chemical pressure effect on the ground state in this Ce_3TiPn_5 system.

Previously, several Hf_5Sn_3Cu-anti type La_3TmPn_5 (Tm denotes the transition metal, and Pn represents pnictogen) materials with well-separated face-sharing octahedral $TmPn_6$ chains have been discovered, where it is focused on the one-dimensional magnetism arising from the magnetic atoms of Tm [21–25]. Now, we try to replace the non-magnetic La atoms in La_3TmPn_5 with magnetic Ce atoms and select the non-magnetic Ti as the transition metal to explore new materials of Ce_3TiPn_5 to study the Ce-derived heavy fermion behavior. Here, we report the new Ce-based compound of Ce_3TiAs_5, where a magnetic transition occurs at 13 K. It is a heavy Fermion compound with a Sommerfeld coefficient about 215 mJ/(Ce-mol*K2). The CEF and magnetic scattering are suggested to be the origin of the hump features in the resistivity. Our results suggest that the ground state of Ce_3TiAs_5 is dominated by RKKY interaction.

2. Experiments

Polycrystalline sample of Ce_3TiAs_5 was synthesized through solid-state reaction method under high-pressure and high-temperature conditions. Ce lumps (Alfa, 99.9%), Ti powder (Alfa, 99.99%) and As powder (Alfa, 99,99%) were used as starting materials. First, the precursor CeAs was prepared by heating the mixture of Ce pieces and As powder at 700 °C for 10 h in an evacuated quartz tube. Then, the obtained CeAs was mixed with Ti and As powders with the molar ratio of 3:1:2. At last, the mixtures were grounded and pressed into pellets and heated at 5 GPa and 1300 °C for 40 min by using a cubic anvil high-pressure apparatus, after which black polycrystalline samples of Ce_3TiAs_5 can be obtained.

The powder x-ray diffraction experiments were conducted on a Rigaku Ultima diffractometer with monochromatic Cu–Kα1 radiation. The DC magnetization measurement was conducted on a Quantum Design Magnetic Property Measurement System. The electrical resistivity was measured by using the typical four-probe method. Both the electrical resistivity and the heat capacity measurements were carried out on a Physical Property Measurement System.

3. Results and discussion

Figure 1(a) shows the x-ray diffraction patterns and the Rietveld refinements for polycrystalline sample of Ce_3TiAs_5. All the peaks can be indexed by a hexagonal structure with $a = b = 8.901$ Å and $c = 5.859$ Å. The Rietveld refinements were performed by adopting the crystal structure of Ce_3TiSb_5 with the space group of $P6_3/mcm$ as the initial model [19], which smoothly converged to $R_p = 6.8\%$, $R_{wp} = 7.5\%$ for Ce_3TiAs_5. The obtained crystallographic data are summarized in table 1. Figure 1(b) presents the sketch of the crystal structure of Ce_3TiAs_5 viewed from the c axis. It can be seen that the structure consists of face-sharing octahedral $TiAs_6$ chains along the c axis, which are arranged to form a triangular lattice in the ab-plane and are separated by zig-zag like Ce-chains. The nearest Ti-Ti distance in the $TiAs_6$ chain is $c/2 = 2.929$ Å; it is much smaller than that of inter-chains given by $a = 8.901$ Å, thus displaying a quasi-one-dimensional (quasi-1D) structure. The Ce atoms are located on the 6 g site and form zig-zag like Ce-chains. The unit cell volume is about 402 Å^3, which shrinks by about 22% relative to Ce_3TiBi_5.

Figure 2(a) displays the temperature dependence of susceptibility for Ce_3TiAs_5 sample measured in zero field cooling (ZFC) and FC modes with an applied external field of 1000 Oe. At low temperature, the susceptibility sharply increases and a bifurcation of ZFC and FC curves can be observed, demonstrating a ferromagnet-like transition. To determine the transition temperature, we plotted the curve of dχ/dT versus temperature as shown in figure 2(b), where the transition temperature can be clearly determined to be ~13 K by the peak of dχ/dT. By using the Curie–Weiss (CW) formula $1/\chi = (T - \theta)/C$, a fitting has been carried out for the data of inverse of susceptibility in high temperature region as shown in figure 2(a). The Weiss temperature $\theta = -55$ K and effective moment $\mu_{eff} = 2.76\ \mu_B$/Ce can be obtained; the negative value of θ indicates a predominated AFM coupling between Ce^{3+} in this compound and the effective moment is close to the value of

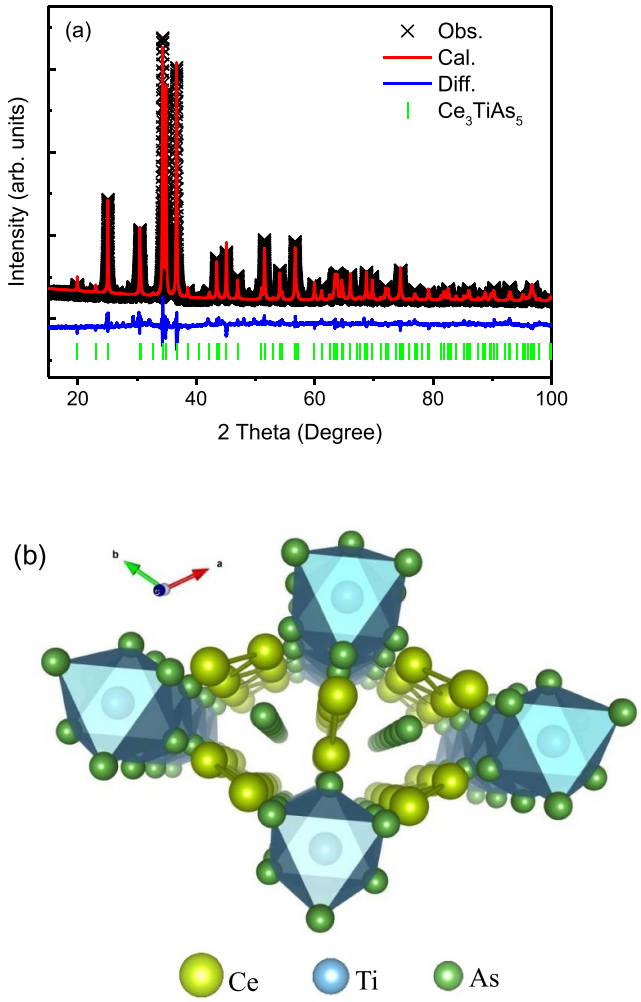

Figure 1. (a) The x-ray diffraction pattern and its rietveld refinement for polycrystalline sample of Ce_3TiAs_5. (b) The sketch of the crystal structure viewed along the *c* axis.

2.54 μ_B for a free Ce^{3+} ion. Below ∼150 K the $1/\chi$ curve gradually deviates from the CW law, which should be mainly attributed to the CEF effect. Such a CEF effect on the deviation of susceptibility from CW law is a general phenomenon for Ce-based compounds [15, 26].

Figure 2(c) shows the isothermal magnetization curves for Ce_3TiAs_5 sample measured at 2 K. It can be seen that a metamagnetic transition occurs at ∼0.7 T. Similar metamagnetic transition also has been observed at ∼4.8 T for Ce_3TiBi_5 [16] and two transitions at ∼0.7 T and 1.1 T for Ce_3TiSb_5 [15]. At the highest applied external field of 7 T, the magnetization approaches a saturated state and the saturated moment is about 0.94 μB/Ce, which is much smaller than that of the fully ordered state of a free Ce^{3+} (2.14 μB/Ce). The reduced saturated moment should arise from the combining contributions of CEF effect and Kondo shielding effect. In addition, a clear hysteresis loop can be observed before the metamagnetic transition with a coercive field ∼1200 Oe as seen in the inset, indicating the existence of ferromagnetic component.

Figure 2(d) displays the temperature dependence of the heat capacity $C(T)$ of Ce_3TiAs_5 and La_3TiAs_5. The magnetic transition is further confirmed by the peak at ∼13 K. The inset shows the C/T versus T^2 plot. A fitting was done for the data by using the equation of $C/T = \gamma + \beta T^2$, where γ and β are the coefficients of the electron and lattice contributions to the heat capacity, respectively. The γ value is obtained to be ∼215 mJ/(Ce-mol*K^2), indicating a heavy fermion behavior. The fitted value of β is ∼0.00137 J/mol-K^4, from which the Debye temperature Θ_D of Ce_3TiAs_5 can be estimated to be 233 K by the formula of $\Theta_D = (12\pi^4 Rn/5\beta)^{1/3}$, here $n = 9$ is the number of atoms in the unit cell. The upturn below 4 K is presented as seen from the inset of figure 2(d). The low temperature upturn in heat capacity usually can be observed and is considered to arise from Schottky anomaly due to a small gap split by CEF effect. Here, it is possible that this upturn behavior is related with heavy fermion effect. When temperature decreases below 4 K, the *c–f* coupling might become strong enough that coherent Kondo scattering emerges, which would make the electron effective mass increase sharply and thus the γ value be quickly enhanced.

The magnetic heat capacity C_m can be obtained by subtracting the lattice contribution from Ce_3TiAs_5, where the heat capacity of La_3TiAs_5 is used as the lattice contribution. Figure 2(e) presents the temperature dependence of C_m. The heat capacity jump due to the magnetic transition is about 1.2 J/(Ce-mol*K), which is nearly one third of the value of 3.9 J/(Ce-mol*K) reported in Ce_3TiSb_5 [15]. The magnetic entropy S_m change can be estimated by integrating C_m/T from 2 K to 30 K. This change of S_m reaches at 50%, 61% and 100% of $R\ln(2S + 1)$ at ∼11 K, T_N and 22 K, respectively, where R is the gas constant and $S = 1/2$ is the effective spin for a doublet ground state. This implies that the magnetic transition occurs in a double degenerated ground state, and the Kondo temperature is roughly evaluated to be 11 K if ignoring the entropy change below 2 K.

Figure 3(a) displays the temperature dependence of resistivity for Ce_3TiAs_5. With decreasing temperature, the resistivity monotonically decreases down to 2 K and drop rapidly corresponding to the magnetic transition. The inset shows the $d\rho/dT$ versus temperature, which of the peak is centered at 13 K and in agreement with the T_N value determined from the magnetic susceptibility and heat capacity measurements. The resistivity at 300 K is ∼ 0.153 mΩ*mm, three times larger than that of La_3TiAs_5 [24]. The larger resistivity of Ce_3TiAs_5 relative to La_3TiAs_5 is considered to be caused by magnetic scattering between Ce-*f* moments and the conducting electrons. The room temperature resistivity reported for single crystal samples of Ce_3TiBi/Sb_5 is in the magnitude of 10–50 μΩ*mm [14, 15, 20]. The very high resistivity of Ce_3TiAs_5 relative to Ce_3TiBi/Sb_5 is supposed to come from the grain boundaries contribution since the polycrystalline samples were used to carry out the resistivity measurements. In addition, there is a minimum reflecting the Kondo effect at about 20–25 K in the resistivity of Ce_3TiBi/Sb_5, while the resistivity minima cannot be observed for Ce_3TiAs_5. It is possible that the resistivity

Table 1. Crystallographic data for Ce_3TiAs_5.

Ce_3TiAs_5 Hexagonal ($P6_3/mcm$)						
$a = b = 8.901(3)$ Å, $c = 5.859(2)$ Å, V = 402.0(3) Å^3						
$R_p = 6.8\%$, $R_{wp} = 7.5\%$						
Atom	Wyck.	x	y	z	Occ.	Uiso
Ce	6 g	0.6182(1)	0	0.25	1	0.005(4)
Ti	2b	0	0	0	1	0.005(4)
As(1)	6 g	0.2511(7)	0	0.25	1	0.005(3)
As(2)	4d	0.33333	0.66666	0	1	0.006(1)

minima might have been masked by the large resistivity due to the grain boundaries contribution.

Figure 3(b) presents the resistivity contributed by magnetic scattering, which is obtained by subtracting the resistivity of La_3TiAs_5 from Ce_3TiAs_5. Obviously, there are two drops in the ρ_m curve at about 150 K and 30 K, which lead to two broad humps in the resistivity of Ce_3TiAs_5 as seen in figure 3(a). In the Kondo system, the degeneracy of the CEF ground state also could be estimated from the magnetic resistivity by using the model proposed by Cornut and Coqblin [27]. In this model, the resistivity is proposed to be proportional to -Ln(T) and the slope proportional to (a_i^2-1) in the case of $\xi_i \ll k_BT \ll \xi_{i+1}$, where ξ_i is CEF splitting energy level and a_i is the total degeneracies of the occupied levels. By using such a relation between the slope and the degeneracy, the degeneracy of the CEF ground state has been estimated to be 2 for CePdGa, which is a reasonable value and agrees with their neutron scattering results [28]. However, we cannot use the theory model to estimate the degeneracy of the CEF ground state for Ce_3TiAs_5 because both the resistivity data for La_3TiAs_5 and Ce_3TiAs_5 were measured from polycrystalline samples.

The hump temperature T_{h1} ~150 K coarsely matches with the temperature where the magnetic susceptibility starts to deviate from the CW law. This high-temperature hump can be explained by the synergy between the CEF effect and magnetic scattering. That is, the CEF effect would lead to a degeneracy lift of the Ce-4f energy levels and the excited energy levels Δ/K_B are usually below 300 K [26, 29, 30]. When temperature decreases crossover Δ/K_B, the Ce-4f electrons would gradually transfer from the up-lying excited energy level to the low-lying energy level. Since the low-lying energy level is a little further away from the Fermi surface relative to the up-lying energy one, the Ce-4f electrons on the low-lying energy level should have weaker exchange interaction with conducting electrons, i.e. a weaker magnetic scattering. Thus, the resistivity would undergo a fast decrease when temperature decreases crossover Δ/K_B and lead to the hump behavior. Therefore, the hump temperature T_{h1} reflects the split excited energy level due to CEF effect.

The low-temperature hump with T_{h2} ~ 30 K should be related with another small excited energy level split by CEF other than the formation of coherent Kondo scattering. First, the Kondo temperature about 11 K estimated from magnetic entropy, below which coherent Kondo scattering usually emerges, is much lower than the hump temperature T_{h2}. Second, negative MR is observed below T_{h2} as seen in figure 3(c). Magnetic field can suppress the Kondo scattering both in incoherence and coherence. Because incoherent Kondo scattering enhances the resistivity while coherent scattering makes the resistivity decrease, negative MR and positive MR are generally observed in the two cases, respectively [31–35]. Here, the negative MR below the low-temperature hump indicates that the drop of ρ_m below 30 K in figure 3(b) cannot be ascribed to the formation of coherent scattering. In addition, according to the increase tendency of S_m with temperature in figure 2(e) with the slope about 0.25 mJ/(Ce-mol*K^2), slightly larger than the obtained γ value due to the Schottky anomaly, the change of S_m would reach RLn 4 at ~44 K, which of the temperature is comparable with T_{h2}. This implies that the first excited CEF doublet should not be at too high temperature. Therefore, it is speculated that the low-temperature hump should arise from the interplay between CEF effect (generating another small excited energy level) and magnetic scattering as well, which is consistent with that two excited energy levels are generated due to the CEF for Ce^{3+} with the site symmetry of $m2m$ in Ce_3TiSb_5 [15]. Similar two humps in resistivity have also be reported to be caused by the interplay of magnetic scattering and the two excited energy levels due to CEF in $CePt_3Si$ [26]. It should be noticed that according to [36], the hump temperature defined from the resistivity is about 0.42 times the CEF excitation energy (Δ/K_B) in the case of a doublet-doublet splitting.

4. Discussions

The discovery of the new compound of Ce_3TiAs_5 can enable us to study the chemical pressure effect on the CEF splitting and AFM temperature T_N in the system of Ce_3TiPn_5 (Pn = Bi, Sb and As). Figure 4(a) presents the anion dependence of lattice parameters. In the sequence of Bi, Sb and As, the lattice parameters monotonically decrease and the unit cell volumes shrink by about 7%, 22% relative to Ce_3TiBi_5, respectively. Figure 4(b) shows the temperature dependence of normalized resistivity (ρ/ρ_{300K}) for Ce_3TiPn_5 (Pn = Bi, Sb and As). The data of Ce_3TiBi_5 and Ce_3TiSb_5 are extracted from [14, 15]. For these compounds, the resistivity curves show quite similar behaviors, such as two humps feature and quick drop due to the magnetic ordering. As above discussion, the high-temperature hump is caused by the interplay between the

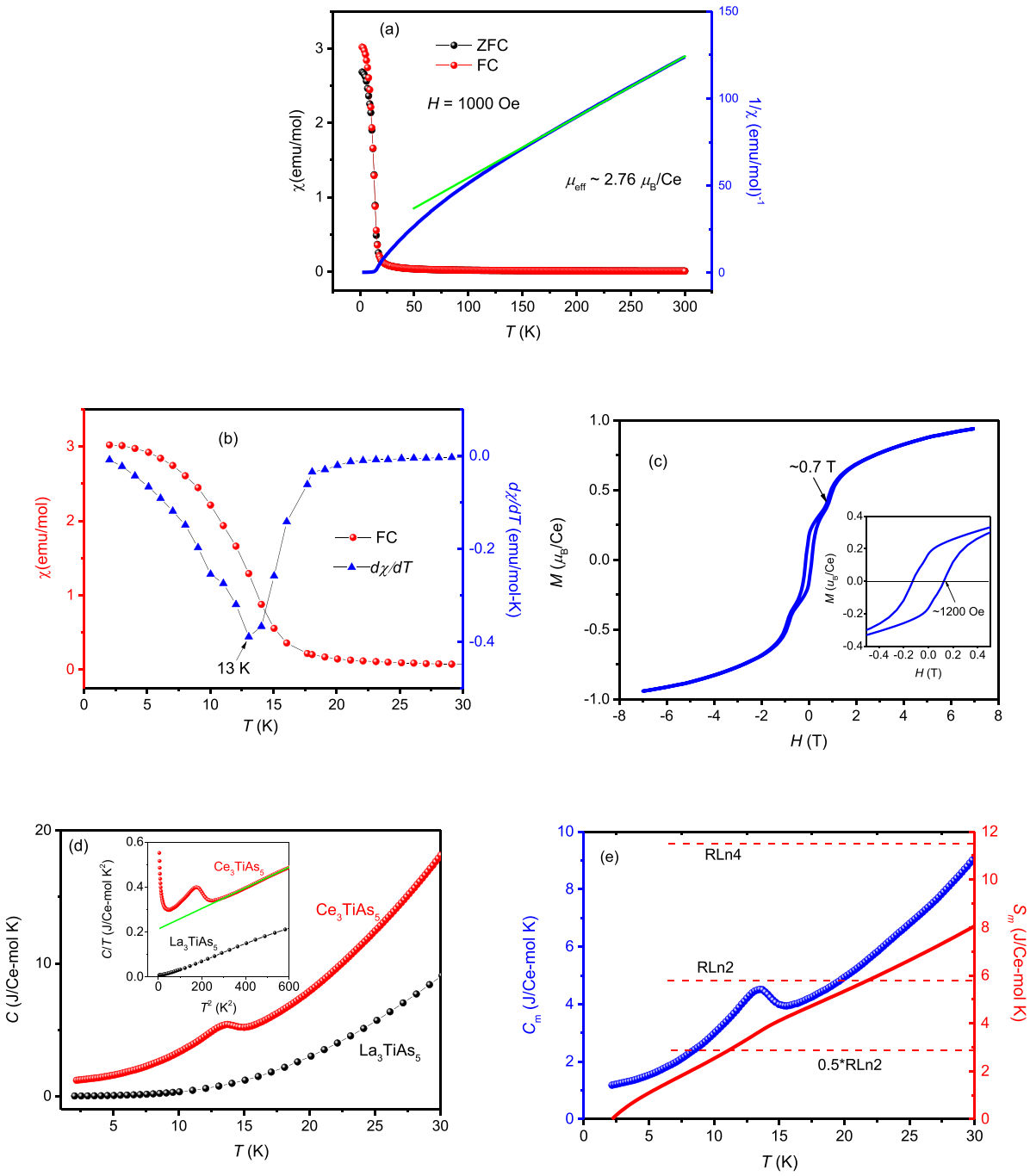

Figure 2. (a) The temperature dependence of magnetic susceptibility measured in zero-field cooling (ZFC) and field cooling (FC) conditions with an applied external field of 1000 Oe. The blue curve shows the reversed susceptibility versus temperature. The green line is the CW fitting. (b) The temperature dependence of susceptibility and the $d\chi/dT$ curves in an enlarged view. (c) The isothermal magnetization curve (M-H) measured at 2 K. The inset shows the enlarged view of the M-H curve to show the coercive field. (d) The temperature dependence of heat capacity $C(T)$ for Ce_3TiAs_5 and La_3TiAs_5. The inset shows the C/T versus T^2. (e) The magnetic heat capacity and the entropy change due to the magnetic transition.

CEF and magnetic scattering and the temperature reflects the excited energy level split by CEF. We can roughly determine the hump temperature T_{h1} by the intersection point between the two tangents of the hump as shown in figure 4(b). The T_{h1} values monotonously increase from 96 K to 150 K when the anion varies from Bi to As. It is a natural result that Ce_3TiPn_5 with small size of anions has short distances of Ce–Pn, and thus a larger CEF effect and leads to a higher T_{h1}. For Ce_3TiBi_5 and Ce_3TiSb_5, negative MR has also been observed below the low-temperature hump [15, 16], which suggests that the two compounds have the same origin of the interplay of CEF effect and magnetic scattering as that in Ce_3TiAs_5.

To study the chemical pressure effect on the magnetic transition, we plotted the T_N versus the shrink of unit cell volume

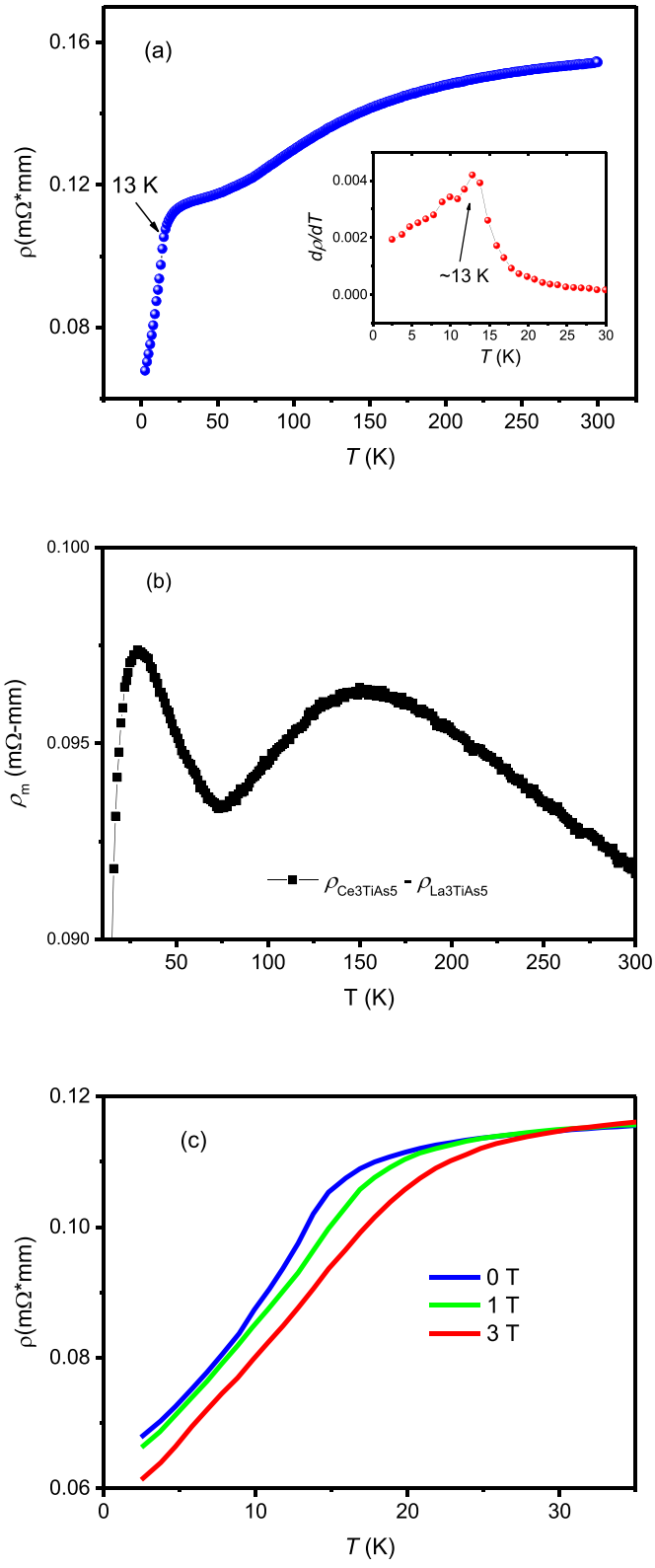

Figure 3. (a) Temperature dependence of resistivity for Ce_3TiAs_5 sample. The inset shows the dρ/dT versus temperature in the low temperature region. (b) Temperature dependence of ρ_m obtained after subtracting the resistivity of La_3TiAs_5 from Ce_3TiAs_5, plotted in a logarithmic temperature scale. (c) The resistivity measured under different magnetic fields.

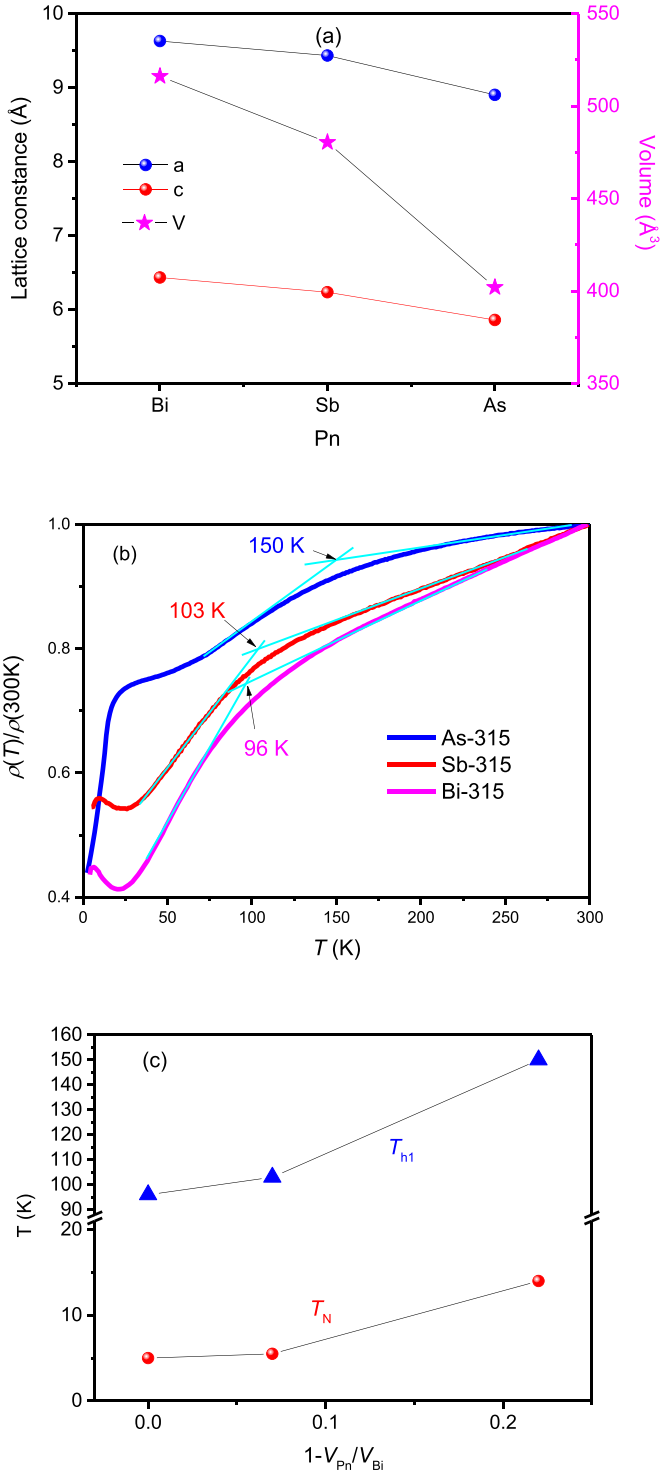

Figure 4. (a) The lattice parameters and unit cell volume of $Ce_3Ti(As/Sb/Bi)_5$. (b) Temperature dependence of normalized resistivity (ρ/ρ_{300K}) for Ce_3TiPn_5 (Pn = Bi, Sb and As). (c) The T_N and T_{h1} versus (1-V_{Pn}/V_{Bi}).

relative to Ce_3TiBi_5 as shown in figure 4(c). It is clearly seen that the T_N monotonously increases in the sequence of Ce_3TiPn_5 with Pn = Bi, Sb and As. It is well known that in the

Ce-based heavy Fermion system, the ground state is governed by the competition between RKKY interaction and Kondo effect, and both of them are associated with the *c-f* coupling J_0. The RKKY interaction usually facilitates the formation of magnetic order while the Kondo effect tends to shield the local spin moment and lead to a nonmagnetic state. The increase of T_N in Ce_3TiAs_5 indicates that RKKY interaction is predominant for the samples of Pn = Bi, Sb and As. We note that the physical pressure effect on the magnetic ordering for Ce_3TiBi_5 has been studied within 8 GPa [20]. T_N is found to increase first with increasing pressure up to 6 GPa and then decrease above this pressure. The highest T_N is about 10 K, lower than Ce_3TiAs_5 (13 K). The different maximum T_N tuned by physical and chemical pressure implies that besides increasing J_0 the replacement of the anion may also have significant effect to change the electric density of state near Fermi level to modify the strength of RKKY.

Since the crystal structure of Ce_3TiPn_5 consists of face-sharing octahedral $TiPn_6$ chains, Pn-chains and zig-zag like Ce-chains along the *c* axis, it is expected that these compounds would have anisotropic physical properties. For Ce_3TiBi_5, the resistivity along the *c* axis $\rho^{//c}$ has been reported to be six times smaller than the in-plane $\rho^{//ab}$ [14], demonstrating an anisotropy of resistivity at ambient pressure. Under high pressure, the high temperature resistance $\rho^{//c}$ shows -Ln(T) dependent, implying that Kondo scattering has played a dominated contribution to the resistance [20], which of the phenomenon has been confirmed by our another work [37]. Further, it has been demonstrated that under pressure the Kondo effect can be ignored for high temperature $R^{//ab}$ [37], which suggests an anisotropic Kondo effect in Ce_3TiBi_5 under high pressure. Considering Ce_3TiAs_5 can be considered as the high pressure state of Ce_3TiBi_5, it is expected that Ce_3TiAs_5 would host anisotropic Kondo effect and deserves to be investigated in the future.

5. Conclusion

A new Ce-based compound Ce_3TiAs_5 has been successfully synthesized under high-pressure and high-temperature conditions, which is isostructural to Ce_3TiBi_5 and Ce_3TiSb_5 with the space group of $P6_3/mcm$. Ce_3TiAs_5 undergoes a magnetic transition at T_N = 13 K, and it exhibits a heavy Fermion behavior with the Sommerfeld coefficient γ = 215 mJ/(Ce-mol*K^2). The two humps in the resistivity curve are indicative of the interplay between the CEF and magnetic scattering effects. Ce_3TiAs_5 has the maximum T_N among the reported Ce_3TiPn_5 family, implying that RKKY interaction is dominant in the system. Since Ce_3TiAs_5 is featured with quasi-1D structure, it would host anisotropic Kondo effect and deserves to be investigated in the future.

Data availability statement

All data that support the findings of this study are included within the article (and any supplementary files).

Acknowledgment

We are grateful to Professor Y F Yang for the useful discussions. This work was supported by the National Key R&D Program of China and the Natural Science Foundation of China under Grants Nos. 2023YFA1406001, 12004161, and 12274193, the Stable Support Plan Program of Shenzhen Natural Science Fund under Grant No. 20200925152415003, the Basic and Applied Basic Research Foundation of Guangdong Province under Grant No. 2022A1515010044. J L Zhu and Y L also acknowledged the Major Science and Technology Infrastructure Project of Material Genome Big-science Facilities Platform supported by Municipal Development and Reform Commission of Shenzhen. Some experiments are supported by the Synergic Extreme Condition User Facility.

ORCID iDs

J F Zhang https://orcid.org/0000-0001-7922-0839
X C Wang https://orcid.org/0000-0001-6263-4963

References

[1] Steglich F, Aarts J, Bredl C D, Lieke W, Meschede D, Franz W and Schafer H 1979 Superconductivity in the presence of strong pauli paramagnetism $CeCu_2Si_2$. *Phys. Rev. Lett.* **43** 1892
[2] Pfleiderer C 2009 Superconducting phases of f-electron compounds *Rev. Mod. Phys.* **81** 1551
[3] Steglich F 2014 Heavy fermions: superconductivity and its relationship to quantum criticality *Phil. Mag.* **94** 3259
[4] von Löhneysen H, Rosch A, Vojta M and Wölfle P 2007 Fermi-liquid instabilities at magnetic quantum phase transitions *Rev. Mod. Phys.* **79** 1015
[5] Wirth S and Steglich F 2016 Exploring heavy fermions from macroscopic to microscopic length scales *Nat. Rev. Mater.* **1** 16051
[6] Shen B *et al* 2020 Strange-metal behaviour in a pure ferromagnetic Kondo lattice *Nature* **579** 51
[7] Patil S *et al* 2016 ARPES view on surface and bulk hybridization phenomena in the antiferromagnetic Kondo lattice $CeRh_2Si_2$ *Nat. Commun.* **7** 11029
[8] Ren Z, Pourovskii L V, Giriat G, Lapertot G, Georges A and Jaccard D 2014 Giant overlap between the magnetic and superconducting phases of CeAuSi under pressure *Phys. Rev.* X **4** 031055
[9] Sun P J and Steglich F 2013 Nernst effect: evidence of local Kondo scattering in heavy fermions *Phys. Rev. Lett.* **110** 216408
[10] Joukovski E, Tugushev V and Avignon M 1999 Weak antiferromagnetism in the Kondo lattice *Physica* B **259** 225
[11] Movshovich R, Graf T, Mandrus D, Thompson J D, Smith J L and Fisk Z 1996 Superconductivity in heavy-fermion $CeRh_2Si_2$. *Phys. Rev.* B **53** 8241
[12] Mathur N D, Grosche F M, Julian S R, Walker I R, Freye D M, Haselwimmer R K W and Lonzarich G G 1998 Magnetically mediated superconductivity in heavy fermion compounds *Nature* **394** 39
[13] Hegger H, Petrovic C, Moshopoulou E G, Hundley M F, Sarrao J L, Fisk Z and Thompson J D 2000 Pressure-induced superconductivity in quasi-2D $CeRhIn_5$. *Phys. Rev. Lett.* **84** 4986

[14] Motoyama G, Sezaki M, Gouchi J, Miyoshi K, Nishigori S, Mutou T, Fujiwara K and Uwatoko Y 2018 Magnetic properties of new antiferromagnetic heavy-fermion compounds, Ce_3TiBi_5 and $CeTi_3Bi_4$ *Physica* B **536** 142

[15] Matin M, Kulkarni R, Thamizhavel A, Dhar S K, Provino A and Manfrinetti P 2017 Probing the magnetic ground state of single crystalline Ce_3TiSb_5 *J. Phys.: Condens. Matter* **29** 145601

[16] Motoyama G, Shinozaki M, Nishigori S, Yamaguchi A, Aso N, Mutou T, Manago M, Fujiwara K, Sumiyama A and Uwatoko Y 2023 Transport, Thermal, and Magnetic Properties of Heavy Fermion Compound Ce_3TiBi_5 *JPS Conf. Proc.* P 011084

[17] Gauthier N, Sibille R, Pomjakushin V, Fjellvag Ø S, Fraser J, Desmarais M, Bianchi A D and Quilliam J A 2024 Magnetic structure of Ce_3TiBi_5 and its relation to current-induced magnetization *Phys. Rev.* B **109** L140405

[18] Ritter C, Pathak A K, Filippone R, Provino A, Dhar S K and Manfrinetti P 2021 Magnetic ground states of Ce_3TiSb_5, Pr_3TiSb_5 and Nd_3TiSb_5 determined by neutron powder diffraction and magnetic measurements *J. Phys.: Condens. Matter* **33** 245801

[19] Moore S H D, Deakin L, Ferguson M J and Mar A 2002 Physical properties and bonding in RE_3TiSb_5 (RE = La, Ce, Pr, Nd, Sm) *Chem. Mater.* **14** 4867

[20] Tsubouchi M, Motoyama G, Gouchi J, Miyoshi K, Nishigori S, Fujiwara K Mutou T and Uwatoko Y 2020 Temperature–pressure magnetic phase diagram of Ce_3TiBi_5 *JPS Conf. Proc.* vol 30 p 011102

[21] Duan L *et al* 2020 High-pressure synthesis, crystal structure and physical properties of a new Cr-based arsenide La_3CrAs_5 *Sci. China Mater.* **63** 1750

[22] Duan L *et al* 2022 Synthesis, structure, and magnetism in the ferromagnet La_3MnAs_5: well-separated spin chains coupled via itinerant electrons *Phys. Rev.* B **106** 184405

[23] Duan L *et al* 2024 Suppression of ferromagnetism in La_3CrAs_5 via V substitution *J. Magn. Magn. Mater.* **589** 171583

[24] Duan L, Zhang J, Wang X C, Zhao J F, Cao L P, Li W M, Deng Z, Yu R Z, Li Z and Jin C Q 2020 High-pressure synthesis, structure and properties of new ternary pnictides La_3TiX_5 (X = P, As) *J. Alloys Compd.* **831** 154697

[25] Zhang C W, Wang Y X, Zheng J X, Du L, Li Y, Han X, Liu E K, Wu Q S and Shi Y G 2024 Crystal growth, transport, and magnetic properties of quasi-one-dimensional La_3MnBi_5 *Phys. Rev. Mater.* **8** 034402

[26] Takeuchi T *et al* 2004 Magnetism and superconductivity in a heavy-fermion superconductor, $CePt_3Si$ *J. Phys.: Condens. Matter* **16** L333

[27] Cornut B and Coqblin B 1972 Influence of the crystalline field on the Kondo Effect of alloys and compounds with cerium impurities *Phys. Rev.* B **5** 4541–61

[28] Adroja D T, Rainford B D and Malik S K 1994 Magnetic transport and neutron scattering studies on ternary equiatomic compound CePdGa *Physica* B **194** 169–70

[29] Nakayama M, Kimura N, Aoki H, Ochiai A, Terakura C, Terashima T and Uji S 2004 Fermi surface and magnetic properties of CeTe *Phys. Rev.* B **70** 054421

[30] Hayashi Y, Takai S, Matsumura T, Tanida H, Sera M, Matsubayashi K, Uwatoko Y and Ochiai A 2016 Kondo effect in CeX (X = S,Se, Te) studied by electrical resistivity measurements under high pressure *J. Phys. Soc. Japan* **85** 034704

[31] Trovarelli O, Geibel C, Cardoso R, Mederle S, Borth R, Buschinger B, Grosche F M, Grin Y, Sparn G and Steglich F 2000 Low-temperature properties of the Yb-based heavy-fermion antiferromagnets YbPtIn, YbRhSn, and YbNiGa *Phys. Rev.* B **61** 9467

[32] Xie W *et al* 2022 Semimetallic Kondo lattice behavior in YbPdAs with a distorted kagome structure *Phys. Rev.* B **106** 075132

[33] Kuthanazhi B, Jo N H, Xiang L, Bud'ko S L and Canfield P C 2022 Magnetisation and magneto-transport measurements on CeBi single crystals *Phil. Mag.* **102** 542

[34] Aronson M C, Thompson J D, Smith J L, Fisk Z and McElfresh M W 1989 Kondo coherence in UBe_{13}: magnetoresistance at high pressure *Phys. Rev. Lett.* **63** 2311

[35] Friedemann S *et al* 2010 Magnetic and electronic quantum criticality in $YbRh_2Si_2$ *J. Low Temp. Phys.* **161** 67

[36] Gopal E 1966 *Specific Heat at Low Temperatures* (Plenum Press)

[37] Fu L C *et al* 2024 Magnetic properties and Kondo effect in Ce3TiBi5 under high pressure Unpublished